# A Novel Test Structure for Process Control Monitor for Un-Cooled Bolometer Area Array Detector Technology

R. S. Saxena, R. K. Bhan, C. R. Jalwania, and S. K. Lomash

*Abstract*—**This paper presents the results of a novel test structure for process control monitor for un-cooled IR detector technology of microbolometer arrays. The proposed test structure is based on resistive network configuration. The theoretical model for resistance of this network has been developed using 'Compensation' and 'Superposition' network theorems. The theoretical results of proposed resistive network have been verified by wired hardware testing as well as using an actual 16x16 networked bolometer array. The proposed structure uses simple two-level metal process and is easy to integrate with standard CMOS process line. The proposed structure can imitate the performance of actual fabricated version of area array closely and it uses only 32 pins instead of 512 using conventional method for a 16x16 array. Further, it has been demonstrated that the defective or faulty elements can be identified vividly using extraction matrix, whose values are quite similar(within the error of 0.1%), which verifies the algorithm in small variation case(~1% variation). For example, an element, intentionally damaged electrically, has been shown to have the difference magnitude much higher than rest of the elements(1.45 a.u. as compared to ~ 0.25 a.u. of others), confirming that it is defective. Further, for the devices having non-uniformity ≤ 10%, both the actual non-uniformity and faults are predicted well. Finally, using our analysis, we have been able to grade(pass or fail) 60 actual devices based on quantitative estimation of non-uniformity ranging from < 5% to > 20%. Additionally, we have been able to identify the number of bad elements ranging from 0 to > 15 in above devices.**

*Index Terms*—**IR detector, Bolometer, Test Structure, Process Control Monitor, Un-cooled**

## I. INTRODUCTION

Uncooled IR detectors based on MEMS metal bolometers are used in thermal imaging applications [1,2]. This technology is maturing fast primarily because of its low cost and compatibility with standard Si CMOS process line. The CMOS process is used for the fabrication of compatible Read Out Integrated Circuit (ROIC).

Among various possible metals, many workers have used Ti [3-4] because of its low thermal conductivity and high TCR. Tanaka et. al. [3-4] were the first to report the fabrication of un-cooled bolometer focal plane array (FPA) using Ti metal resistors and an array of MOS switch network for accessing individual elements. Butler [5] reported bolometric FPA with an integrated signal processor. Excellent reviews on theory, fabrication and system aspects were published by Wood [6] and Kruse et. al.[7]. Development of microbolometer detector using CMOS n-well layer as IR material was reported by Sabuncuoglu et. al.[8]. Eriksson et. al.[9] used pre-fabricated ROIC as a substrate for their bolometric FPA and provided detailed results on thermal characterization of membrane structures. They also used pre-fabricated BiCMOS ROIC for their un-cooled FPA. Tanaka et. al. [10] reported influence of bias heating using Ti bolometer. The structures proposed and used by above authors were good starting examples, however, these studies were either single element based or MOS switch based(for arrays). Former

Manuscript received July 4, 2006; revised Sep. 26, 2006.
Solid State Physics Laboratory, Lucknow Road, Delhi-110054 (India)
E-mail : rs_saxena/sspl@ssplnet.org

approach is not true replica of actual array environment while later approach necessitates fabrication of large circuitry and can test only the combined performance (ROIC switch + bolometer) of the detector element. Another possible test structure using linear array lacks the effect of area environment.

To circumvent above problems, we are proposing in this paper, a simple and novel resistance network based Process Control Monitor (PCM) test structure that uses only one interconnect bus per row or column and addresses the above issues. This amounts to only 32 connections for an array of 16x16 compared to 512 using conventional approach. It uses two-level metal process and is easy to integrate with standard CMOS process line. This PCM is particularly useful for yield prediction for actual large sized arrays. Here, we shall show that using this structure, one can identify faulty/defective elements and correlation is good between theory and experiment.

Section 2 discusses the newly proposed resistive network. Section 3 is about the theory and verification of extraction algorithm using dummy hardware. Section 4 discusses briefly bolometer array fabrication details and experiments done on those arrays to verify the effectiveness of algorithm. Section 5 shows results and discussions on arrays fabricated in our laboratory and in section 6 we summarize the conclusions.

## II. Double Metal Layer Based Resistive Network

A simple resistance network structure using two levels of metal lines, crossing perpendicularly to each other (just like rows and columns) is shown in Fig. 1. The fabrication details are given in section 4.

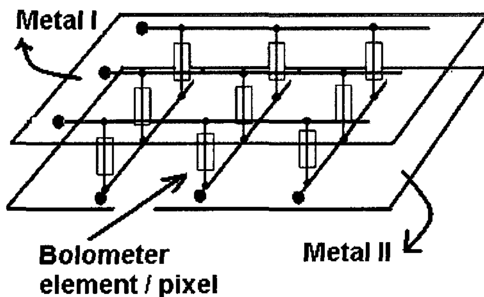


**Fig. 1.** Connection scheme of bolometer elements in the array.

Each bolometer element has been shown connected to two levels of metal interconnect buses wherein one of its ends is connected to one metal line (say column line) and other end to its cross line (row line). The advantage of this configuration is single pad is being used for all the elements of one row/column, which reduces the number of pads required for accessing all the bolometer elements. This minimizes the fan-out metal tracks and allows one to accommodate this structure into the PCM easily, primarily due to small Si real estate requirements and very easy layout.

Though this structure is easy to implement, it has got the undesired networking effect. While accessing one element, all others form a network in parallel with it. Therefore, the individual behavior of the element is modified. To get rid of this unwanted networking effect, we developed a method for extracting the actual resistance of the individual elements from networked measurement data as discussed in the paper.

## III. Theory

This section describes a theoretical model for effective resistance of the network so that we may extract the actual resistances from the measured resistance values. We analyze the structure by applying a constant current between the nodes where we want to measure the resistance. The voltage developed across these nodes gives the measure of resistance if we divide it by the current applied.

Fig. 2 shows the resistor array of 4x4 format for illustration purpose. However, the model has been developed for the general case of NxN array. Initially,

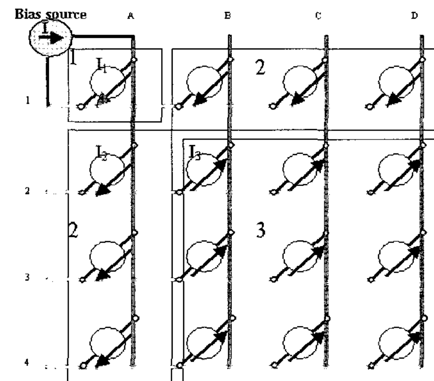


**Fig. 2.** Schematic of 4x4 bolometer array in network configuration.

for bias point analysis we assume that all the elements in the array have equal resistances (R) at a given temperature. Practically, elements may have some differences in their values. These differences will be taken into account in the small variation analysis by assuming that the elements are changing their resistances one by one to attain their final values. Effect of resistance change (ΔR) in one element will be analyzed and it will be shown later that individual effects may be superimposed to find the overall effect of non-uniformity by virtue of linear nature of resistive networks.

All the elements of the array may be sub-divided into three zones (as indicated in the fig. 2) based on their circuital symmetry.

1. Zone-1: Single element directly connected to the bias source.
2. Zone-2: 2(N-1) elements having only one end directly connected to the bias source, i.e., elements lying on either the same row or the same column where the bias source is connected.
3. Zone-3: $(N-1)^2$ elements not directly connected to the bias source.

Next the currents flowing in these zones will be calculated leading to calculations of the effective resistance of the network.

### 1. Bias Point Analysiss

Referencing to Fig. 2, a current source injecting a current of I is applied between A and 1. Let, the current flowing from A to 1, via direct path is $I_1$. Now, the nodes 2, 3, 4 have circuital symmetry, therefore the currents from A to 2, A to 3 and A to 4 will be the same (say $I_2$). Similarly, nodes B, C, D have circuital symmetry. Hence, current from any of 2, 3, 4 to any of B, C, D will be the same (say $I_3$). Also, the current $I_2$ will be recollected at nodes B, C and D. The total current I is given by

$$I = I_1 + (N-1)I_2 \tag{1}$$

where, N is number of elements in a row/column. Further, the current $I_2$ is being divided equally in (N-1) parts, each having value $I_3$. Hence,

$$I_3 = \frac{I_2}{(N-1)} \tag{2}$$

Now equating the potential drop from nodes A to 1 via two different paths (Path1: Directly from node A to node 1, Path2: node A to node 2, node 2 to node B and node B to node 1) we get, $RI_1 = RI_2 + RI_3 + RI_2$ and therefore $I_1 = 2I_2 + I_3$. Now using equation (2) we get

$$I_1 = \frac{(2N-1)I_2}{(N-1)} \tag{3}$$

Hence, by above relations, we get

$$I_1 = \frac{(2N-1)I}{N^2} \tag{4.1}$$

$$I_2 = \frac{(N-1)I}{N^2} \tag{4.2}$$

$$I_3 = \frac{I}{N^2} \tag{4.3}$$

The important information that we may extract from these equations is that the ratio of bias currents for 'Zone 1 element', 'Zone 2 elements' and 'Zone 3 elements' is:

$$I_1 : I_2 : I_3 = (2N-1) : (N-1) : 1 \tag{5.1}$$

Another important information that we get in bias point analysis is the equivalent resistance in networked resistor array between one row and one column node. If the equivalent resistance between node A and node 1 is $R_{eq}$, then the potential drop from node A to node 1 will be $R_{eq}I$. From equation (4.1), one can infer that this potential drop is also equal to $RI_1$. Therefore, we get $R_{eq}I = RI_1$, which leads to

$$R_{eq} = R\frac{(2N-1)}{N^2} \tag{5.2}$$

This $R_{eq}$ is the effective equivalent resistance of networked-element (1, 1). The value given by equation (5.2) is theoretically estimated resistance for ideal case where all the resistors have same resistance R. If we

measure resistance between all combinations (of one row and one column), we shall get the complete 'measured data matrix'. That matrix can be used for estimating the extraction data, which will be used for determining the faulty elements as will be shown in the later sections.

## 2. Small Variation Analysis

In practical situation, the resistances of bolometers may vary over the array even with well-controlled process. Therefore, in this section we try to develop an analysis for small variation case. Ultimately, we shall derive a method to find the actual variation of resistances using measured data. Since the network is resistive, it will follow the linearity and homogeneity. This allows us to use ***Superposition Theorem*** [11] for finding the effect in $R_{eq}$. due to small variations in more than one individual element.

Let us assume that R changes by an amount ΔR at any random location in the array. Further, let us chose the location as intersection point between node C and node 3, as shown in Fig. 3. Now according to the ***Compensation Theorem*** [11], all the changes in current and voltages in the network may be found by first replacing all the energy sources by their internal resistances and then putting a current source in parallel with the element under consideration. Therefore, we replace the bias current source by its internal resistance (Infinite, i.e., open circuit) and connect a current source $I_C$, between node C and node 3 as shown in Fig. 3. The value of this compensation current, according to the theorem is given by:

$$I_C = \frac{\Delta R . I_b}{(R + \Delta R)} \qquad (6)$$

where $I_b$ is the bias current through the element that has undergone the resistance change, named here as 'element under consideration' (EUC) and $I_C$ is the compensation current.

Now, without loss of originality, we can replace column A with column C and also row 1 with row 3 as shown in Fig. 4. One may compare the Fig. 4 with Fig. 2. Both are quite similar except that the current source is

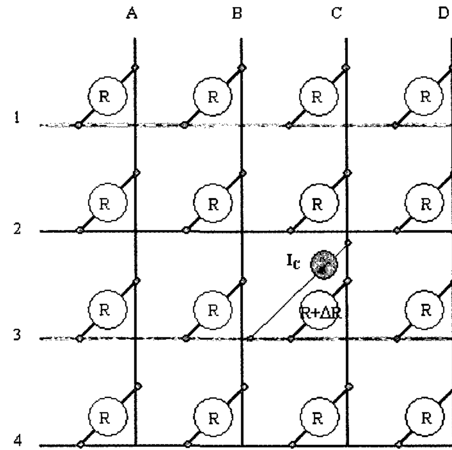


**Fig. 3.** The resistance change of R modeled using compensation theorem.

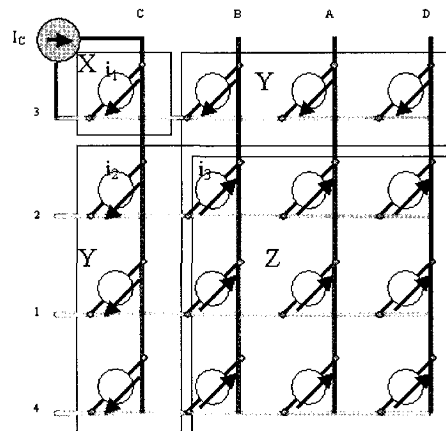


**Fig. 4.** Interchanging the columns A and C and rows 1 and 3 in figure 3.

now a compensation source and one resistance value is slightly different (by ΔR) than others.

Here also the zones may be defined based on the circuital symmetry. As shown in Fig. 4, elements in zone Y and Z will have the small variation-currents $i_2$ and $i_3$ respectively whereas zone X contains only one element with variation-current $i_1$. It should be noted here that $i_1$, $i_2$ and $i_3$ are the variation in currents in the respective elements due to small variation in the resistance at location (3, C) and should not be confused with the bias currents $I_1$, $I_2$ and $I_3$ discussed in section 3.1. Now, again by circuit analysis we get:

$$I_C = i_1 + (N - 1) i_2 \qquad (7)$$

Further, the current $i_2$ is being divided equally in (N-1) parts. Hence,

$$i_3 = \frac{i_2}{(N-1)} \tag{8}$$

Now equating the potential drop from C to 3 via two different paths (similar to the Bias Point Analysis discussed in section 3.1) we get $i_1(R+\Delta R) = i_2 R + i_3 R + i_2 R$ , which leads to the following relation.

$$i_1 = \left(\frac{(2N-1)}{(N-1)}\frac{R}{(R+\Delta R)}\right)i_2 \tag{9}$$

Hence, by relations (7) and (9), we get

$$I_C = \left[\left(\frac{(2N-1)R}{(N-1)(R+\Delta R)}\right) + (N-1)\right]i_2$$

After performing simple algebra and re-arrangement, we get

$$i_2 = \frac{(N-1)(R+\Delta R)}{\left(RN^2 + \Delta R(N-1)^2\right)} I_C \tag{10.1}$$

Similarly, one can solve these equations for $i_1$ and $i_3$ to find the following relations

$$i_1 = \frac{(2N-1)R}{\left(RN^2 + \Delta R(N-1)^2\right)} I_C \tag{10.2}$$

$$i_3 = \frac{(R+\Delta R)}{\left(RN^2 + \Delta R(N-1)^2\right)} I_C \tag{10.3}$$

Now, substituting the value of $I_C$ from equation (6), into the equation set (10) we get:

$$i_1 = \frac{(2N-1)R}{\left(RN^2 + \Delta R(N-1)^2\right)} \frac{\Delta R}{(R+\Delta R)} I_b \tag{11.1}$$

$$i_2 = \frac{(N-1)(R+\Delta R)}{\left(RN^2 + \Delta R(N-1)^2\right)} \frac{\Delta R}{(R+\Delta R)} I_b \tag{11.2}$$

$$i_3 = \frac{(R+\Delta R)}{\left(RN^2 + \Delta R(N-1)^2\right)} \frac{\Delta R}{(R+\Delta R)} I_b \tag{11.3}$$

Here, the value of bias current, $I_b$, depends on the zone of the EUC and will be determined using the bias point analysis discussed earlier. For measuring $i_1$, we put the current source across EUC and then EUC falls in zone 1 of Fig. 2, causing $I_b = I_1$. Similarly, for determining $i_2$ and $i_3$, we get the value of $I_b$ to be $I_2$ and $I_3$ respectively. Therefore, from equation sets (4) and (11) we get:

$$i_1 = \frac{(2N-1)R}{\left(RN^2 + \Delta R(N-1)^2\right)} \frac{\Delta R}{(R+\Delta R)} \frac{(2N-1)}{N^2} I \tag{12.1}$$

$$i_2 = \frac{(N-1)(R+\Delta R)}{\left(RN^2 + \Delta R(N-1)^2\right)} \frac{\Delta R}{(R+\Delta R)} \frac{(N-1)}{N^2} I \tag{12.2}$$

$$i_3 = \frac{(R+\Delta R)}{\left(RN^2 + \Delta R(N-1)^2\right)} \frac{\Delta R}{(R+\Delta R)} \frac{1}{N^2} I \tag{12.3}$$

Hence, utilizing above obtained variational currents and knowing the resistance values (for each element in the present case, except element (3, C)) leads to change in voltages $\Delta v1$, $\Delta v2$, and $\Delta v3$ corresponding to three different zones.

$$\Delta v1 : \Delta v2 : \Delta v3 = (2N-1)^2 : (N-1)^2 : 1 \tag{13}$$

Till now, we assumed that only one resistance is subjected to slight change ($\Delta R$) in its value. But, in practice all the NxN resistances may change. These *resistance-changes* are represented here as $r_{11}, r_{12} \ldots r_{NN}$. So, if we bias the circuit by connecting a constant current source (supplying current I) between one column node and one row node, and the elements undergo the changes in their resistances, we shall see the change in voltage on those nodes. These changes in voltage will lead to the change in apparent resistance, denoted by ($\Delta R^{eq}$). If the changes in individual resistances are small, the $\Delta R^{eq}$ will be obtained by simply superimposing all the individual effects. Hence, we derive the following equation.

$$\Delta R_{1,1}^{eq} = K\left\{(2N-1)^2 r_{11} + (N-1)^2 \sum_{i=2}^{N} r_{1i} + (N-1)^2 \sum_{i=2}^{N} r_{i1} + \sum_{i=2}^{N}\sum_{j=2}^{N} r_{ij}\right\} \tag{14}$$

Here, $\Delta R_{1,1}^{eq}$ is the change in equivalent (measured) resistance between column 1 and row 1. K is the constant that depends on the value of N. The

approximate value of K can be determined from the equation set (12), which will be

$$K \sim \frac{1}{N^4} \tag{15}$$

For every set of nodes (one row and one column), we get the similar equations. In this way, we get $N^2$ equations for $N^2$ variables. These may be solved to find the relative values of resistance changes.

If we take N=16 in equation (14) and add up the weight terms, we get 961, for (1, 1) location, 225 for (1, 2) and so on. Following the same logic, all the weight coefficients are shown in $W_{1,1}$ weight matrix as follows

$$W_{1,1} = \begin{bmatrix} 961 & 225 & 225 \ldots\ldots\ldots\ldots 225 \\ 225 & 1 & 1 \ldots\ldots\ldots\ldots 1 \\ & & \\ & & \\ 225 & 1 & 1 \ldots\ldots\ldots\ldots 1 \end{bmatrix} \tag{16}$$

The similar weight coefficient matrices, i.e., $W_{a,b}$: a = {1 to 16}; b = {1 to 16}, may be constructed if we analyze other 255 locations. Therefore, there will be a total of 256 equations. These weight coefficients represent the modification of basic resistances due to networking effect (set of $N^2$ simultaneous equations) as they appear in equation (14). The computation of these weight coefficients will finally allow us to extract the values of individual resistances, if they were un-networked similar to usual FPA mode.

In short, the effect of parallel networking on a particular bolometer element can be estimated and simple resistance measurement between all set of two nodes (one row and one column) will allow us to calculate the original resistance values.

### 3. Experimental Verification of Algorithm

The algorithm based on the above-discussed theory has been implemented in MATLAB6.5. We tested and verified it on a 4x4 array of 1 K ohm resistors (within 1% tolerance), assembled according to Fig. 1.

The actual values of various resistors are shown in table 1 with mean value of 994.77ohm. The resistance

**Table 1.** The resistances of resistors forming 4x4 network along with 2D map.

| | | | |
|---|---|---|---|
| 993.09 | 994.79 | 993.66 | 993.52 |
| 994.53 | 995.40 | 995.81 | 996.69 |
| 993.38 | 996.14 | 995.92 | 995.97 |
| 994.94 | 993.66 | 995.39 | 993.35 |

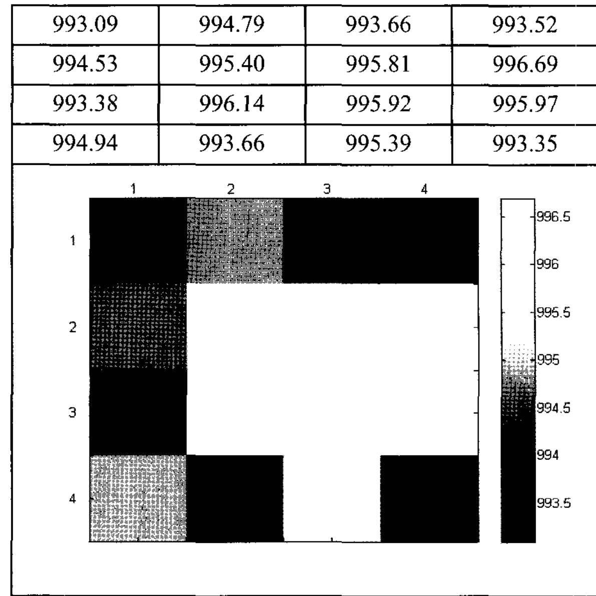


measurement was performed with HP-3457A Multimeter, using a well-known 'Kelvin' technique. According to the theory, the apparent resistances should be 435.21 ohm (equation 5.2). As we shall see in the subsequent sections, we actually get the same values, conforming the theory. The 2D intensity map (table 1) graphically depicts the non-uniformity of the resistance values. The magnitude of variation may be found using the scale shown on the right side.

Now, we deliberately introduced some changes to these resistances and show that the changes introduced may clearly be predicted by the extracted data. These changes and their effects have been discussed in the following sections with following cases.

- **Case1**: Normal networking of all the resistors
- **Case2**: Networking with one high resistance
- **Case3**: Networking with one location short circuited
- **Case4**: Networking with one short and one open circuited (high resistance) locations
- **Case5**: Networking with one resistor deviating by 10 % of its resistance.

Table 2(a) shows the resistance measurement data and its intensity map for case 1. These values are between 434.61 ohm to 435.50 ohm as expected from theory. The total variation of 3.6 ohm in original values has been reduced to only 0.89 ohm due to networking

**Table 2.** Measured and extracted resistances (in ohm) and intensity maps for case 1.

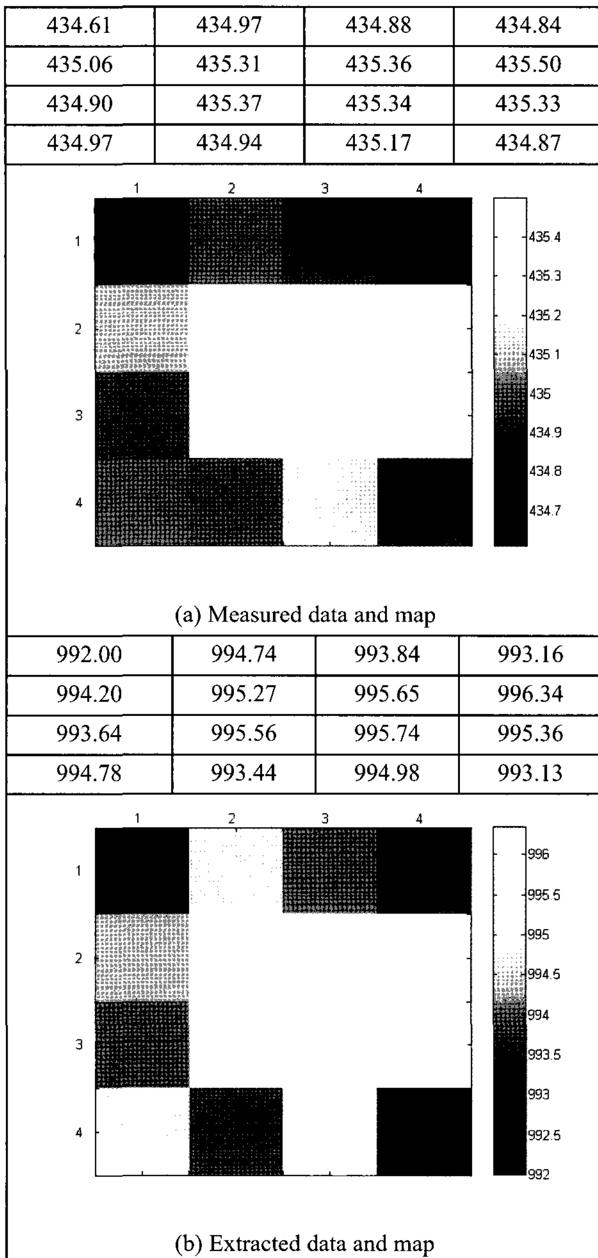

| 434.61 | 434.97 | 434.88 | 434.84 |
|---|---|---|---|
| 435.06 | 435.31 | 435.36 | 435.50 |
| 434.90 | 435.37 | 435.34 | 435.33 |
| 434.97 | 434.94 | 435.17 | 434.87 |



(a) Measured data and map

| 992.00 | 994.74 | 993.84 | 993.16 |
|---|---|---|---|
| 994.20 | 995.27 | 995.65 | 996.34 |
| 993.64 | 995.56 | 995.74 | 995.36 |
| 994.78 | 993.44 | 994.98 | 993.13 |



(b) Extracted data and map

**Table 3.** Measured and extracted resistances (in ohm) and intensity maps for case 2.

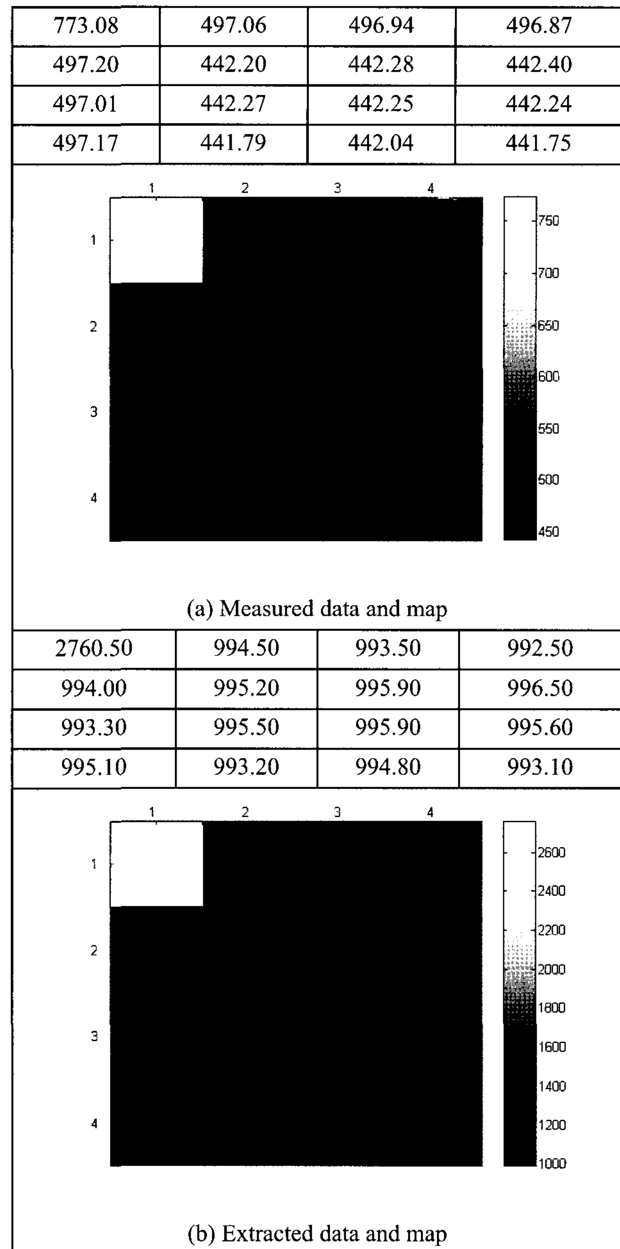

| 773.08 | 497.06 | 496.94 | 496.87 |
|---|---|---|---|
| 497.20 | 442.20 | 442.28 | 442.40 |
| 497.01 | 442.27 | 442.25 | 442.24 |
| 497.17 | 441.79 | 442.04 | 441.75 |



(a) Measured data and map

| 2760.50 | 994.50 | 993.50 | 992.50 |
|---|---|---|---|
| 994.00 | 995.20 | 995.90 | 996.50 |
| 993.30 | 995.50 | 995.90 | 995.60 |
| 995.10 | 993.20 | 994.80 | 993.10 |



(b) Extracted data and map

effect. The extracted data from algorithm is shown in table 2(b) along with its 2D intensity map. The original and extracted values of table 1 and table 2(b) respectively are quite similar (within 0.1% error), thus verifying the algorithm in ~1% variation case.

Now, we open circuited one element (case 2) at location (1, 1) and not disturbed any other element. The resistance data and extraction results are shown in table 3.

By examining the intensity maps of table 3, one may directly pinpoint the element (1, 1) to be faulty. Further, it may be seen that the other elements of row 1 and column 1 have also become gray in 4(a) because of the networking. Table 3(b) may still clearly distinguish the faulty location without any ambiguity. Again, as a case 3, we short-circuited the resistor at location (1, 1). The results are summarized in table 4. Here also, the intensity map helps to identify correctly the fault.

To see the effect of two different faults simultaneously on a single array, the location (1, 1) is short-circuited and location (4, 3) is open circuited (case 4). The extraction results (table 5(b)) clearly show the

**Table 4.** Measured and extracted resistances (in ohm) and intensity maps for case 3.

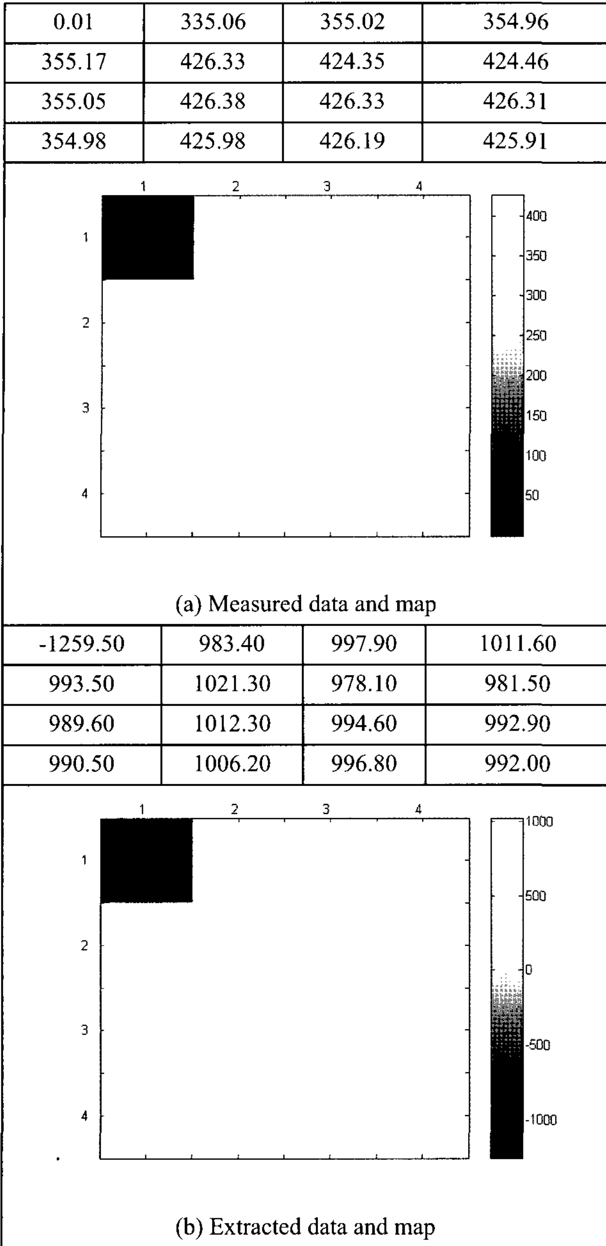

| 0.01 | 335.06 | 355.02 | 354.96 |
|---|---|---|---|
| 355.17 | 426.33 | 424.35 | 424.46 |
| 355.05 | 426.38 | 426.33 | 426.31 |
| 354.98 | 425.98 | 426.19 | 425.91 |



(a) Measured data and map

| -1259.50 | 983.40 | 997.90 | 1011.60 |
|---|---|---|---|
| 993.50 | 1021.30 | 978.10 | 981.50 |
| 989.60 | 1012.30 | 994.60 | 992.90 |
| 990.50 | 1006.20 | 996.80 | 992.00 |



(b) Extracted data and map

**Table 5.** Measured and extracted resistances (in ohm) and intensity maps for case 4.

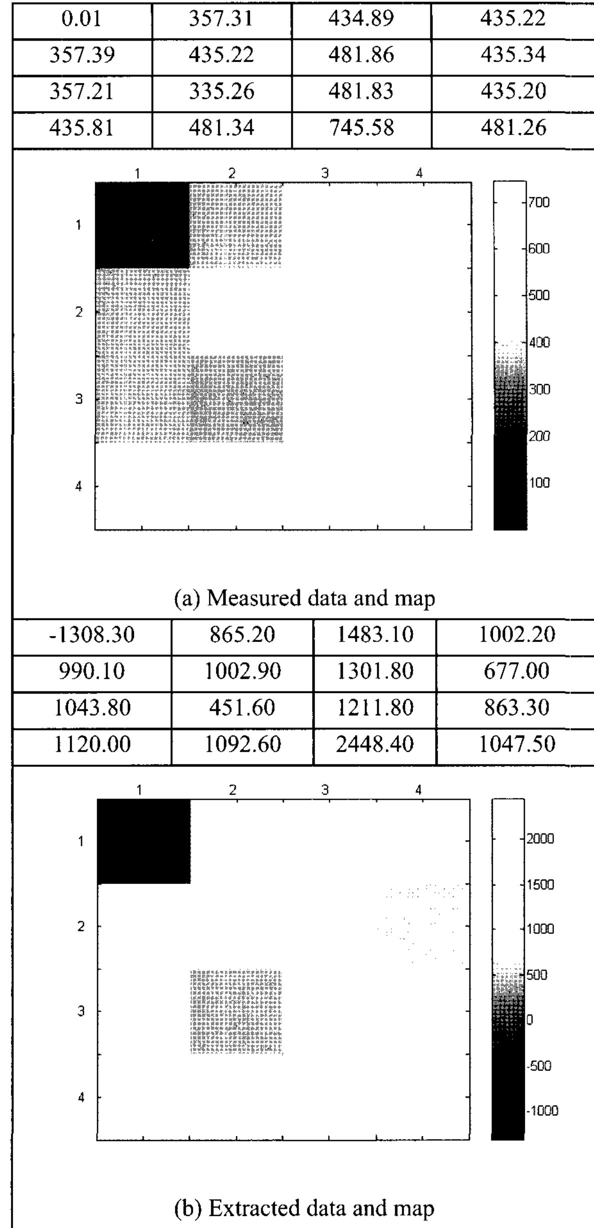

| 0.01 | 357.31 | 434.89 | 435.22 |
|---|---|---|---|
| 357.39 | 435.22 | 481.86 | 435.34 |
| 357.21 | 335.26 | 481.83 | 435.20 |
| 435.81 | 481.34 | 745.58 | 481.26 |



(a) Measured data and map

| -1308.30 | 865.20 | 1483.10 | 1002.20 |
|---|---|---|---|
| 990.10 | 1002.90 | 1301.80 | 677.00 |
| 1043.80 | 451.60 | 1211.80 | 863.30 |
| 1120.00 | 1092.60 | 2448.40 | 1047.50 |



(b) Extracted data and map

faulty elements. In the intensity map the short-circuited element is completely black whereas the open circuited location is white. This proves the effectiveness of the algorithm in determination of faulty elements.

A slight discrepancy is observed in extracted data of above cases. This occurs because we treated the short circuits and open circuits as small variations, which may have some impact on the expressions obtained in the analysis (section 3.2). Still the faulty circuit locations (short or open) are clearly visible in extracted data map.

We kept a resistor of resistance 1098.87 ohm at location (3, 4) and did not disturb any other resistor. The measurement results of table 6 (a) show the location of high resistance element clearly but at the same time the elements of row no. 3 and column no. 4 are also affected. This may lead to misinterpretation of the non-uniformity. Also the 10% variation has been reduced to only about 4% in measured data. This is all due to networking of elements. The intensity map becomes clearer in extracted case as seen in table 6(b) and helps to pinpoint the location without any ambiguity. This is the most practical case we encounter and hence this verifies the

**Table 6.** The measured and extracted resistance values for 10% variation (case 5).

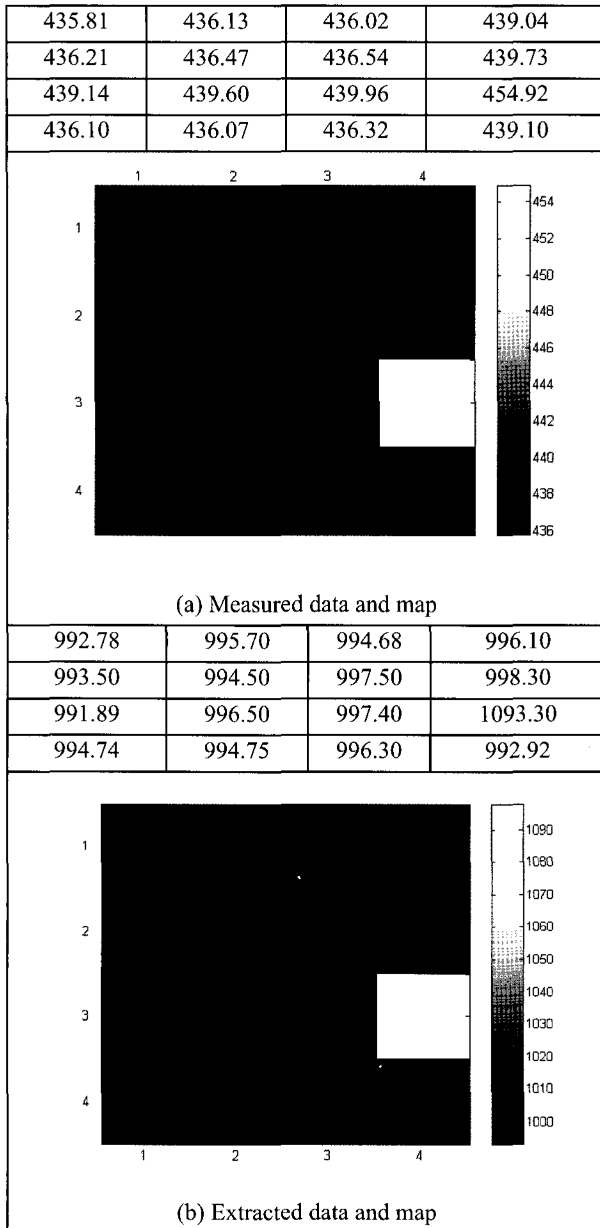


| 435.81 | 436.13 | 436.02 | 439.04 |
|---|---|---|---|
| 436.21 | 436.47 | 436.54 | 439.73 |
| 439.14 | 439.60 | 439.96 | 454.92 |
| 436.10 | 436.07 | 436.32 | 439.10 |

(a) Measured data and map

| 992.78 | 995.70 | 994.68 | 996.10 |
|---|---|---|---|
| 993.50 | 994.50 | 997.50 | 998.30 |
| 991.89 | 996.50 | 997.40 | 1093.30 |
| 994.74 | 994.75 | 996.30 | 992.92 |

(b) Extracted data and map

effectiveness of the algorithm.

In general, the negative values in extracted data indicate the short-circuited locations whereas the excessive positive indicates open circuited (highly resistive) locations. Therefore, first hand look at the extracted data gives the idea of number of faulty elements immediately.

It may be summarized from these results that for non-uniformity below 10%, both the non-uniformity and faults are predicted well by our analysis and for above 20% cases the extraction matrix may not be accurate. These cases are any way not acceptable for thermal imaging applications and are indicative of immature process.

## IV. EXPERIMENT ON THE 16X16 BOLOMETER ARRAY

The PCM test structure has been fabricated in the form of 16x16 array of microbolometers. The extraction algorithm has been implemented on these structures and it is shown by the experiments, that the method may be used effectively to qualify the arrays by determining the non-uniformity in the array. It is also effective to locate the faulty elements, if any.

### 1. Fabrication Details

In this study, standard double metal process of Al has been used for row and column buses. For the bolometer element, it consists of a membrane and its support legs using the microbridge technology. The typical photograph is shown in Fig. 5. The finner details of our fabrication process are given in Ref. [12]. Briefly, a 1.0 μm thick membrane of $Si_3N_4$ is grown on silicon substrate having 2 μm air gap between the membrane and the substrate and supported by two hinges. Following this, bolometers of 700 Angstroms of Ti with Al contacts have been made on these membranes. A variety of devices with various dimensions (for optimization purposes) have been used for the device fabrication. Various small arrays of 16x16 having different hinge length/width/thickness have been fabricated. Here most of the results are reported for 50x50 $\mu m^2$ element dimensions.

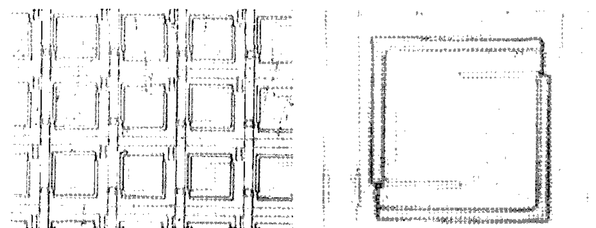

**Fig. 5.** (a) A portion (~3x3) of a typical 16x16 bolometer test structure (b) The detailed zoomed view of one element using Ti metal.

## 2. Implementation of Algorithm

Here, we present the results on an actual array of 16x16 bolometers. Resistance measurements of the 256 elements (in 16x16 network) were carried out using 32 nodes discussed earlier. As said earlier, the primary advantage of this structure is that it just needs 2N pins/pads for testing NxN array, which would otherwise need $N^2$ pins/pads, and yet it imitates the actual array in actual FPA mode using ROIC. So, the conclusions drawn from this mini array will be in general valid for the big arrays (barring yield or scaling up issues if any).

Since the number of readings is large (256) in our case, the results are depicted in two-dimensional intensity map for convenience in Fig. 6. The Fig. shows the resistance map and its extracted data map for our typical array of 16x16 bolometers. A non-uniform array has been selected for better illustration. This non-uniformity in the arrays occurs due to process and material variations and immature technology. This contributes to fixed pattern noise (FPN) of the FPA. We qualify the arrays based on its FPN that should be less than 10%.

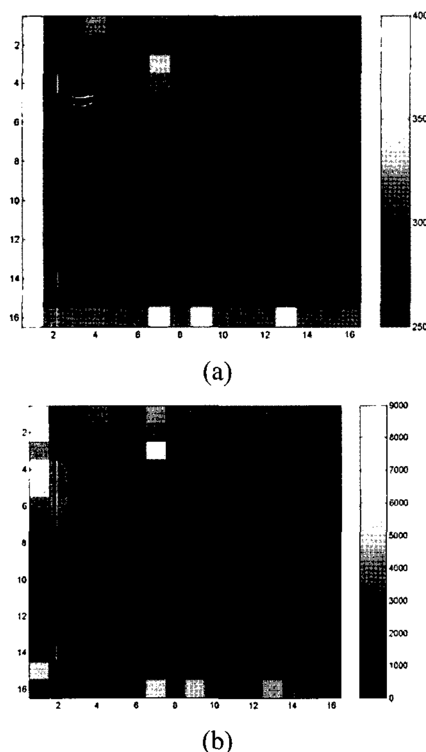

(a)

(b)

**Fig. 6.** The intensity maps of (a) Resistance measurement data (in ohm) and (b) Extracted resistance data (in ohm) of a typical 16x16 bolometer array.

The strips of different intensities are visible in the measurement data in Fig. 6(a). If one element has unusual (high or low as compared to others) resistance, the whole row and column strips are affected. Therefore, the information that one can get using this map is very little and it is hard to make any conclusion about the actual non-uniformity of the array. The only information that may be found from the measurement data map is that some elements in the bright strips will be highly resistive and vise-a-versa.

The extracted map shown in Fig. 6(b) gives the better insight of the array. The elements much away from their design value of 2500 ohm (faulty) are clearly visible. It is clear from Fig. 6 (a) and (b) that some bright elements in 2D map of measured data are not bright in the extracted data map. For example, it appears from the measured data of Fig. 6(a) that all the 16 elements in column 1 have high resistance but by extraction of this data we find that only about 6 elements in column 1 have high resistance. Similar thing is visible in columns 7, 9, 13 and rows 4, 14 and 16. Thus, we find the actual non-uniformity in the array from the extracted data.

## 3. Identification of Faulty Elements

Finally, for experimental correlation with actual devices, we examined the faults under microscope. Since a healthy looking element under microscope may also have some electrical connectivity defect, to verify the algorithm we did an experiment of electrical burning. A fault has been introduced intentionally at any randomly selected location. The location (13, 15) on the same device discussed in section 4.2 was selected as a test case. A current source has been connected between row 13 and column 15 and then a current (2 mA) has been passed through it for a few seconds causing partial damage. The element directly connected between row 13 and column 15 will obviously have the largest damaged as compared to other elements because it allows the maximum current across it. The other elements of the row 13 and column 15 will also get slightly damaged. This was verified by actual measurement shown as 2D map of Fig. 7.

Now, by comparison of damaged and undamaged measurement data, i.e., Fig. s 6(a) and 7(a), we find that the intensity of row and column of the selected element

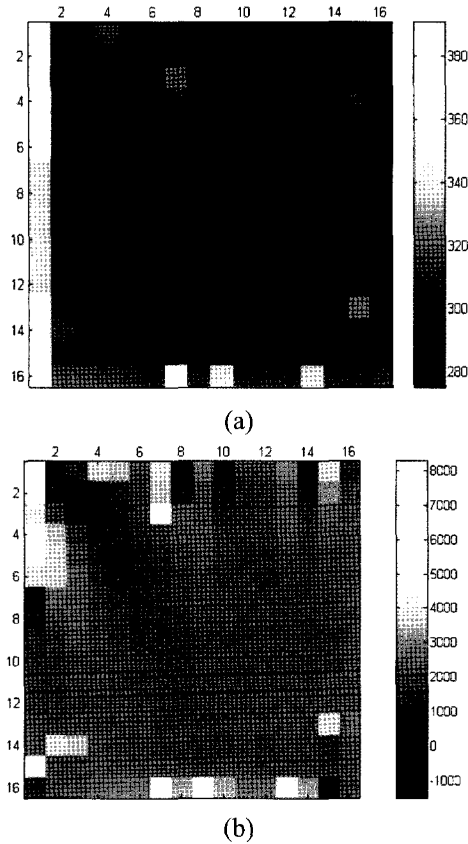


**Fig. 7.** The intensity map of the electrically damaged array (a) Measured, (b) Extracted data.

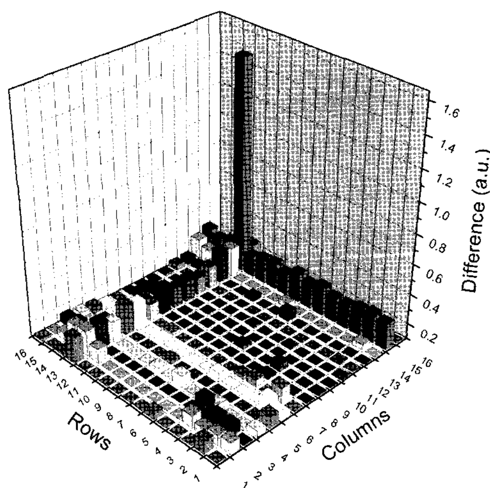


**Fig. 8.** Plot of the difference between extracted data of original and damaged array.

(13, 15) has increased, the maximum being at the element itself, as expected. The extracted data may also be compared using Fig. 6(b) and 7(b). Here also we find that element (13, 15) has the increased intensity and other elements of row 13 and column 15 have also slightly increased intensity.

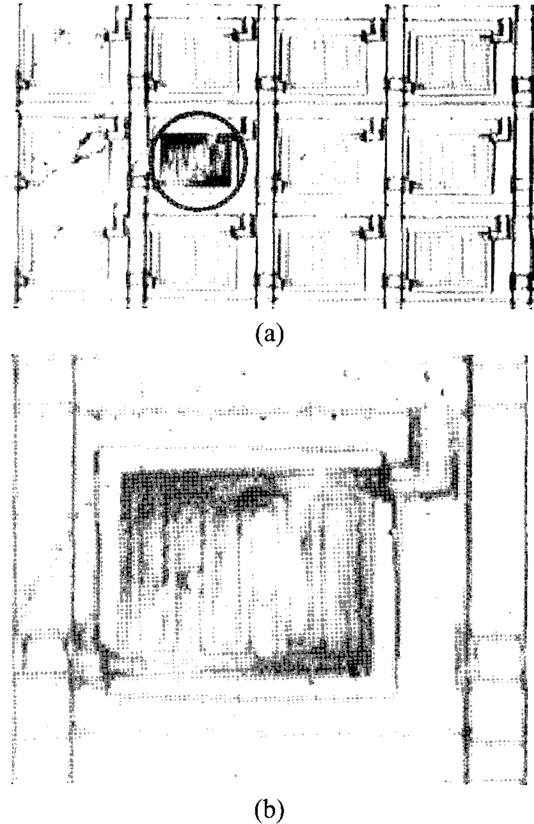

**Fig. 9.** The burned bolometer element (a) In array (b) The enlarged view.

To clearly visualize this effect, the difference between extracted data before damage, shown in Fig. 6(b) and after damage, shown in Fig. 7(b) has been plotted in Fig. 8. The element (13, 15) has the difference magnitude much higher than rest of the elements, confirming its more damage. This is because of local heating due to high current and subsequent burning. Additionally, the other elements of row 13 and column 15 also have moderately high difference values than others as expected.

We correlated this with the health of the element (13, 15) by microscopic examination. Fig. 9a shows the element (13, 15) with its neighboring elements. It may be seen that indeed the element (15, 13) is partially burned and has become black. The amplified view is shown in the Fig. 9b.

Another advantage of extraction is that one gets to know the actual individual values of the elements in the array as if they were isolated. These values can be used for modeling the actual array (non-networked) using ROIC for actual fabrication of bolometer FPAs later.

By using the relay based switching system, one can use our proposed test structure to remove the effect of networking and monitor the performance of the test structure as in actual FPA mode [13]. Thus, we see that the effect of non-uniformity in the resistance values of the bolometer elements translate into variation in extracted data matrix. The assumption of identical resistance values and small variation (<1%) used in the development our theory does not deter one from drawing conclusions about identification of faulty elements whose extracted data varies sufficiently (>10%) and hence are clearly distinguishable in the practical situations.

## V. Results and Discussion

A large number of 16x16 micro-bolometer arrays have been processed and the extraction algorithm has been applied for first stage qualification of the devices before detailed thermal and radiometric characterization.

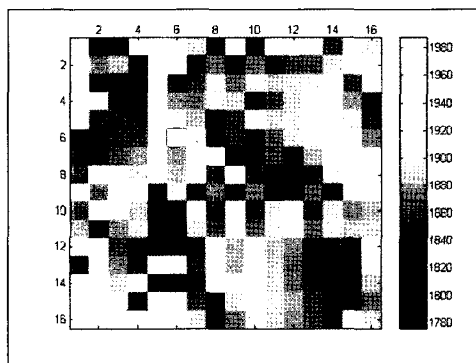


(a)

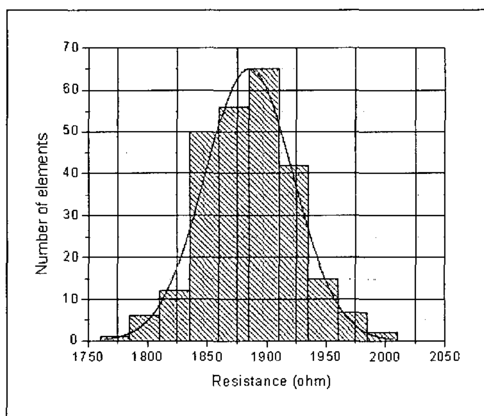


(b)

**Fig. 10.** The results of a typical bolometer array of 10% non-uniformity (a) Extracted 2D intensity map, (b) The histogram of resistance distribution.

The extracted data was plotted in 2D intensity maps and in statistical histograms as shown in Fig. 10 for a typical device having non-uniformity about 10%. 2D map gives the location of the high and low resistive elements whereas histogram provides the distribution of resistance over the array.

It may be seen from the Fig. 10(a) that this particular array has no defective element but has a non-uniformity of 10% and follows an expected normal distribution as depicted in 10(b). This non-uniformity as discussed earlier is due to process variations. Such arrays have been qualified as 'passed' for our process. Devices have been graded according to their performance as discussed below.

Table 7 summarizes the qualification results of resistance measurements (and extraction) on a set of 60 microbolometer arrays tested using our newly proposed algorithm. The devices were graded based on resistance non-uniformity as shown in table 7(a). First and second grade devices were used for detailed characterization and subsequent processing. The devices having non-uniformity more than 10% have been discarded.

The discarded devices, as shown in the table 7, are

**Table 7.** Statistical results of resistance measurement data for 60 arrays (a) Non-uniformity bar chart, (b) Bad elements bar chart.

| Non-Uniformity | Passed | | Failed / Discarded | | |
|---|---|---|---|---|---|
| | Grade 1 NU < 5% | Grade 2 NU = 5-10% | NU = 10-15% | NU = 15-20% | NU > 20% |
| No. of devices | 3 | 12 | 20 | 8 | 18 |

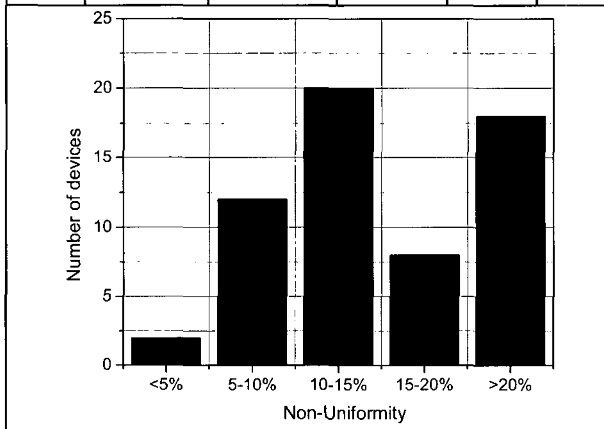


(a)

| 1.1 Bad Elements | 0 | 0-5 | 5-10 | 10-15 | >15 |
|---|---|---|---|---|---|
| 1.1.1.1.1.1.1 No. of devices | 15 | 7 | 13 | 17 | 8 |

(b)

those either having faulty elements (including 'shorts' and 'highly resistive or open') or having non-uniformity variations above 10% of average. Table 7(b) shows the categories of devices based on number of bad elements. Some of the discarded devices were used for destructive measurement for process evaluation and further analysis. For example the device discussed in section 4.3 is one of those.

Finally, we have been able to monitor and control effectively the resistance variation in our arrays in addition to pin pointing the locations of faulty/bad elements.

## VI. CONCLUSIONS

We have presented the theory and experimental results of novel test structure, which can be used as a PCM for initial development of process leading to the fabrication of 2D bolometer IR detector arrays. The structure is based on resistive element network whose resistance behavior is modeled by simple algorithm using Compensation and Superposition network theorems. The theory and experimental results show that such a structure can imitate the actual Bolometer FPA performance as well as help in identifying 'faulty elements' and 'non-uniformity' easily. In addition, it can be easily incorporated into standard CMOS fabrication lines. It has been shown by experimental evidence that our analysis is well suited for identification of faulty elements and measure of non-uniformity. We have applied this algorithm to our bolometer arrays and isolate the bad arrays based on extracted non-uniformity data.

## ACKNOWLEDGMENTS

The authors would like to thank Director, SSPL for permission to publish this work.

## REFERENCES

[1] A. Fraenkel, U. Mizrahi, L. Bykov, A. Adin, E. Malkinson, Y. Zabar, D. Seter, Y. Gebil, And Z. Kopolovich, "Advanced features of SCD's uncooled detectors", *Optoelectronics Review,* Vol. 14(1), pp 47-54, 2006.

[2] Kenneth A. Hay, Dale Van Deusen, Tina Y. Liu, William A. Kleinhans, "Uncooled Focal Plane Array Detector Development at Infrared Vision Technology Corporation", *Proc. SPIE* Vol. 5074, pp 491-499, 2003.

[3] A. Tanaka, N. Teranishi, NEC Japan, "Titanium Bolometer-Type Infrared Detecting Apparatus", *US Patent5698852,* Dec. 16, 1997.

[4] A. Tanaka, S. Matsumoto, N. Tsukamoto, S. Itoh, K. Chiba, T. Endoh, A. Nakazato, K. Okuyama, Y. Kumazawa, M. Hijikawa, H. Gotoh, T. Tanaka and N. Teranishi, "Infrared Focal Plane Array Incorporating Silicon IC Process Compatible Bolometer", *IEEE Trans. Electron Devices,* vol. ED-43, pp1844-1850, 1996.

[5] N. R. Butler, "Bolometric Focal Plane Array", *US Patent 6249002 B1,* 19 Jan, 2001.

[6] R. A. Wood, in "Uncooled Infrared Imaging Arrays and Systems", Ch.3, pp45-119, Eds. P.W. Kruse and D.D. Skatrud, Academic Press, San Diego, USA, 1997.

[7] R. W. Kruse, in "Uncooled Infrared Imaging Arrays and Systems", Ch.2, pp17-42, Eds. P.W. Kruse and D.D. Skatrud, Academic Press, San Diago, USA, 1997.

[8] D.S. Tezcan, S. Eminoglu and T. Akin, "A low-cost uncooled infrared microbolometer detector in standard CMOS Technology", *IEEE Trans. Electron Devices*, vol. ED-50, pp494-501, 2003.

[9] P. Eriksson, J.Y. Anderson, and G. Stemme, "Thermal characterization of surface-micromachined Silicon nitride membranes for thermal infrared detectors", *Microelectromechanical Systems,* vol. 6, pp. 55-61, 1997.

[10] A. Tanaka, S. Matsumoto, N. Tsukamoto, S. Itoh, K. Chiba, T. Endoh, A. Nakazato, K. Okuyama, Y. Kumazawa, M. Hijikawa, H. Gotoh, T. Tanaka and N. Teranishi, "Influence of Bias Heating: Ti Bolometer Infrared Sensor", *SPIE,* vol. 3061, pp198-209, 1997.

[11] D. Roy Choudhury, "Networks and Systems", Ch. 7, pp316-367, Wiley Eastern Limited, New Age International Limited.

[12] V.K. Jain and C.R. Jalwania, "Development of IR sensor using MEMS technology", *Proceedings of the International Conference on Smart Materials,*

*Structures and Systems*, Eds. P.D. Mangalgiri, A.R. Upadhya, A. Selvarajan, Indian Institute of Science, Banglore, Allied Publishers Limited, New Delhi, 1999.

[13] M. C. Torquemada, V. Villamayor, M. T. Rodrigo, G. Vergara, F. J. Sánchez, R. Almazán, M. Verdú, P. Rodríguez, L. J. Gómez, M.T. Montojo, "Polycrystalline PbSe x-y addressed uncooled FPAs" *Proc. SPIE*, vol 5074, p 592, 2003.

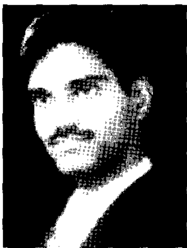

**R. S. Saxena** did his B.E. in Electronics and Communication Engineering from GBPEC, India in 1997. Then he joined as a Scientist in Solid State Physics Laboratory (SSPL), Delhi, in1998. He did M. Tech., in Microelectronics from IIT Bombay in 2003. He is currently a part time research scholar in Electrical Engineering Department at IIT Delhi. He has worked on design, modeling and characterization of various semiconductor devices and also worked on SPICE parameter extraction. He has published about 10 research papers in various reputed journals and conferences. His current fields of interest are mixed signal CMOS VLSI circuits, nanoscale device modeling and simulation and characterization of IR detectors and FPAs.

**R. K. Bhan** has received his M.Sc Degree in Physics from Kashmir University, Srinagar, India in 1982 and Ph.D degree in Physics from Delhi University in 1994. He was initially Junior Research Fellow in "Center for Applied Research in Electronics" at Indian Institute of Technology, New Delhi from 1982 to 1984. He joined Solid State Physics Laboratory, Delhi as a scientist in 1984 where he is currently involved in Infrared Detector characterization. His research interests include MOS physics, CCDs, IR detectors and FPAs. He has published more than 50 research papers in international journals.

**C. R. Jalwania** received his MSc (Physics) degree from University of Rajasthan in 1973. He joined DRDO in 1974 at the Defence Electronics Research Laboratory (DLRL), Hyderabad, India and worked on the development of RADAR antenna in L-band. He has also worked at the Ionospheric Research Station, Guwahati, India. He joined Solid State Physics Laboratory (SSPL) in 1981. His area of research include Solar cells, P-I-N diodes semiconductor bridge as an ignitor for explosives, porous-silicon and microelectromechanical Systems (MEMS) based on micromachining of Si. He has published around 15 research papers in various reputed journal. He has been awarded the best paper in International Workshop on Physics of Semiconductor Devices (IWPSD) held in 1997 in Delhi, India. He has been given the "Technology Award-2005" by DRDO, Min. of Defence, for 16x16 microbolometer array development. Currently he is working on the 32x32 Ti-microbolometer array.

**S. K. Lomash** obtained his M.Sc. (Physics) and Ph.D. degree from Delhi University, Delhi, India, in 1971 and 1976 respectively. Initially, he was lecturer of Physics in a DU college till 1979. After that he moved to Solid State Physics Laboratory, Delhi as a Scientist. He worked on various solid state device fabrication and testing. He has published more than 20 research papers in reputed journals. His current research interests are IR detector technology, MEMS technology and characterization of semiconductor devices.